

Effect of boundary conditions and domain size on the turbulent flow characteristics over a circular cylinder

by Salman Masood

Submission date: 09-Aug-2024 02:43AM (UTC-0500)

Submission ID: 2424771427

File name: the_turbulent_flow_characteristics_over_a_circular_cylinder.pdf (9.83M)

Word count: 9284

Character count: 47925



Effect of boundary conditions and domain size on the turbulent flow characteristics over a circular cylinder

Syed Ahmad Raza, Yosua Heru Irawan & Ming-Jyh Chern

To cite this article: Syed Ahmad Raza, Yosua Heru Irawan & Ming-Jyh Chern (2021): Effect of boundary conditions and domain size on the turbulent flow characteristics over a circular cylinder, Journal of the Chinese Institute of Engineers, DOI: [10.1080/02533839.2021.1940295](https://doi.org/10.1080/02533839.2021.1940295)

To link to this article: <https://doi.org/10.1080/02533839.2021.1940295>



Published online: 14 Jul 2021.



[Submit your article to this journal](#)



Article views: 26






[View related articles](#)



[View Crossmark data](#)



Effect of boundary conditions and domain size on the turbulent flow characteristics over a circular cylinder

Syed Ahmad Raza , Yosua Heru Irawan  and Ming-Jyh Chern 

Department of Mechanical Engineering, National Taiwan University of Science and Technology, Taipei City, Taiwan

ABSTRACT

Numerical investigation of the effects of boundary conditions and computational domain size on simulations of a circular cylinder in three-dimensional (3-D) turbulent flow at $Re = 3900$ has been conducted using a direct-forcing immersed boundary (DFIB) method. The turbulent flow scales were simulated using the Smagorinsky model. Two computational domain sizes and three different sets of boundary conditions were investigated. The results of all the cases were compared against published literature. The study proved the capability of the selected DFIB method for investigating fluid-structure interactions in turbulent flow. It also found that the increase in the size of the computational domain improved the accuracy of the results, especially in the far wake region. Interestingly, switching the lateral boundaries between periodic and symmetry conditions enabled the numerical simulation to approach the two different experimental results.

ARTICLE HISTORY

Received 20 July 2020
Accepted 2 February 2021

KEYWORDS

Direct-forcing immersed boundary method; Smagorinsky model; domain size; boundary conditions

1. Introduction

Numerical simulations of fluid-structure interactions are widely used in science and engineering and even indispensable in many research, design and development applications (Wang et al. 2020; Jang et al. 2019). All numerical studies must identify their region of interest at the outset. Consequently, the size of the computational domain and the appropriate set of boundary conditions must be selected. Selection of a sufficiently large computational domain to minimize any non-physical effects of the numerically imposed boundary conditions is very important, while ensuring that the domain size is still feasible with respect to computational requirements. The boundary conditions themselves have to be applied in a way to ensure the physical integrity of the flow and minimization of any computational artifacts.

Flows over a circular cylinder are a popular choice for investigations because while incorporating a simple geometry, they enable the study of the flow topology around the solid object and shed light on the nature of boundary layer separation as well as the wake and the recirculation region. These types of studies allow general conclusions to be drawn about the suitability of the numerical method adopted for fluid-structure interactions. Furthermore, owing to their widespread engineering applications such as industrial chimneys or bladeless wind turbines, flows over circular cylinders are also important due to their implications specific to various such applications.

Different aspects of the effects of domain size on numerical results have been investigated in the past. Tezduyar and Shih (1991) conducted two-dimensional (2-D) numerical experiments for flow past a cylinder at $Re = 100$ to study the influence of the streamwise domain size by varying the location of the downstream boundary from 2.5 to 25 diameters from the

cylinder center. They found that the downstream boundary could be placed as close 14.5 diameters from the cylinder center with no noticeable difference in the observations. Moreover, even bringing the downstream boundary as close as 6.5 diameters from the cylinder center only caused very minor variations in the solution. They used symmetry boundary conditions (zero normal velocity and zero tangential stresses) at the lateral ends (with respect to flow direction and cylinder; neither streamwise nor spanwise) of the computational domain.

In contrast to Tezduyar and Shih (1991), Behr et al. (1995) investigated the lateral boundaries in their 2-D study of flow past a cylinder at $Re = 100$. They also used symmetry boundary conditions at the lateral boundaries and tested two different types of finite element formulations. They varied the lateral boundary from 4.5 diameters from the cylinder center to 16 diameters and found a dependence of the lateral boundary on the fluid flow characteristics such as Strouhal number (St). However, their chosen computational methods lead to St higher than the experimental value for smaller lateral distances and lower than the experimental value for larger lateral distances, depending on the finite element formulation adopted.

Lei, Cheng, and Kavanagh (2000) conducted numerical experiments to determine the effect of spanwise length of the computational domain for a three-dimensional (3-D) simulation of flow past a cylinder and also compared it to their 2-D simulation. They conducted their study at $Re = 1000$ and varied the spanwise length from zero (for 2-D) to six diameters. Their analysis also included the effect of a turbulence model to account for the small scale instabilities in the flow. In their 3-D simulations, they selected periodic (cyclic) boundary conditions on the spanwise boundaries and symmetry boundary

conditions on the lateral boundaries. As expected, they found that 2-D simulation is not accurate enough for predicting flow parameters at $Re = 1000$. This has been documented in the literature that a 3-D simulation is better suited to account for the three-dimensional vortical structures leading to improved results (Mittal and Balachandar 1997). More importantly, Lei, Cheng, and Kavanagh (2001) observed that even for 3-D flows, a spanwise length of less than 2 diameters could give an inaccurate prediction of the flow but more than 2 diameters spanwise length gave sufficiently accurate results. For further investigation of the effect of spanwise length of the computational domain, Labbé and Wilson (2007) conducted a study for a range of Reynolds numbers from 100 to 1000 with the same boundary conditions as Lei, Cheng, and Kavanagh (2001). They considered the spanwise extensions of $\pi/2D$, πD and $2\pi D$. They concluded that a spanwise length of about 4 diameters was sufficient to predict the flow past an infinitely long circular cylinder for Reynolds numbers of up to 300, whereas an even shorter spanwise length between $\pi/2D$ and πD was sufficient for higher Reynolds numbers. Since they had considered a range of Reynolds numbers, they also predicted that their conclusions may be valid beyond their investigated range exceeding $Re = 1000$. For the spanwise direction, the importance of grid resolution has also been confirmed by Breuer (1998).

Some researchers have also investigated the effect of domain size on CFD simulations of other cases. For example, Rezaeiha, Kalkman, and Blocken (2017) investigated the effect of domain size on CFD simulations of a vertical axis wind turbine. However, other problems are not as comprehensively covered in the published literature. Even for flows past a cylinder which are the most well-documented, there are only a few numerical experiments in the literature that have studied the effect of the size of computational domain and fewer (if any) that have conducted a detailed comparison of the effects of using different boundary conditions.

Fluid flows past a cylinder in the subcritical range ($300 < Re < 3 \times 10^5$) exhibit a laminar boundary layer separation followed by a transition to a turbulent wake. For such flows, $Re = 3900$ is often used as a benchmark due to the availability of multiple experimental and numerical studies. A uniform constant-velocity inlet boundary condition is generally adopted (Breuer 1998). Downstream conditions are not as important as long as they do not cause any reflections or significant disturbances to the flow in the computational domain, especially when vortices pass through the downstream boundary. However, the effect of spanwise and lateral boundary conditions on the flow past a cylinder could be more interesting.

Beaudan and Moin (1994) attempted one of the earliest large eddy simulation (LES) studies of this case. Kravchenko and Moin (2000) numerically investigated the same case using a high-order numerical approach based on Galerkin B -splines method along with a dynamic LES model on an O-type grid with a selected domain size of $60D \times \pi D$. Periodic spanwise boundary conditions were employed but details of the lateral boundary conditions were not given. They compared their results with the earlier experiments by

Lourenco and Shih (1993) (first published in Beaudan and Moin (1994)) and Ong and Wallace (1996). Kravchenko and Moin (2000) have plotted the transverse variation of the mean streamwise velocity at different x/D locations in the wake of the cylinder. They have discussed how the mean streamwise velocity profile changes from a flat-bottomed U-shaped profile at $x/D = 0.58$ near the cylinder to a sharp V-shaped profile at an $x/D = 1.54$. This phenomenon is well-documented in the literature and it reflects how the shear layers transition to turbulence in the wake of the cylinder when the vortex formation takes place.

The relatively U-shaped results of Kravchenko and Moin (2000) for the mean streamwise velocity profile close behind the cylinder at $x/D = 1.06$ did not fully agree with the experimental results of Lourenco and Shih (1993). To explain this difference, they suggested that this difference was due to some external disturbances affecting the experimental setup that caused an earlier transition to turbulence in the shear layers downstream of the cylinder, leading to a shorter region of vortex formation and the V-shaped profile. However, the exact nature of such external disturbances and their reasons were not confirmed.

Parnaudeau et al. (2008) conducted comprehensive experimental and numerical studies for the same case and also attempted to resolve the previous discrepancy between numerical and experimental results. Using hot-wire anemometry and particle image velocimetry, they conducted experiments to find results that differed from previous experimental results and displayed a much more prominent U-shaped mean streamwise velocity profile at $x/D = 1.06$. For their numerical simulations, they used an immersed boundary method (IBM) with LES and periodic boundaries on the lateral as well as spanwise boundaries of the computational domain. The size of their computational domain was $20D \times 20D \times \pi D$. Their experimental and numerical results were in good agreement with each other.

Lysenko, Ertesvåg, and Rian (2012) also reported results for flow over a cylinder at $Re = 3900$ using OpenFOAM toolbox along with Smagorinsky as well as a dynamic k -equation eddy viscosity subgrid scale (SGS) model on an O-type curvilinear grid with a grid size of $50D \times \pi D$. However, their results from the conventional Smagorinsky model (V-shaped) differed greatly from the results obtained using the dynamic k -equation eddy-viscosity SGS model, which were U-shaped.

A parametric study for this case was conducted by Sidebottom, Ooi, and Jones (2015) using different types of turbulence models, wall models, discretization schemes and grid resolutions. They used a computational domain composed of a semi-circular region (of radius $7D$) connected to a rectangular region (length $17D$) with the overall dimensions of $24D \times 14D \times \pi D$. The boundary conditions in the spanwise direction of the cylinder were periodic but the lateral boundary conditions were not specified. They recommended a y^+ of less than 30 as larger values affected the accuracy.

Recently, Pereira et al. (2018) employed Partially-Averaged Navier-Stokes (PANS) equations to investigate the same problem of flow over a circular cylinder with $Re = 3900$. They compared the results for modeling different fractions of the

turbulence kinetic field from 0.15 to 1.0. Their simulation used the QUICK scheme (Leonard 1979) on a $50D \times 24D \times 3D$ grid. Interestingly, they implemented symmetry conditions on the spanwise boundaries because they determined in their earlier work (Pereira, Vaz, and Luís 2015) that neither periodic nor symmetric conditions could optimally account for the non-turbulent instabilities in the spanwise direction. Therefore, they preferred to use the symmetry boundary conditions to lower the numerical cost of periodic conditions. For the lateral boundaries, they opted to use zero-gradient (Neumann) conditions.

The computational domain sizes and boundary conditions used by the various studies for $Re = 3900$ discussed above are given in Table 1. Most researchers have used periodic conditions on the spanwise boundary, except for Pereira et al. (2018). Not much emphasis is placed on the lateral boundaries as several published studies have skipped its description. However, Lei, Cheng, and Kavanagh (2001) ($Re = 1000$) and Labbé and Wilson (2007) ($Re = 100 - 1000$) used symmetry conditions for the lateral boundary and periodic conditions for the spanwise boundary, which have not been explicitly adopted for any of the above studies. The flow parameters from the studies conducted at $Re = 3900$ are given in Table 2.

In the present study, we conduct numerical experiments at $Re = 3900$ for two sets of computational domains and three sets of boundary conditions for the spanwise and lateral boundaries. A description of these cases is given in Table 3. The objective is to determine if the domain size and the choice of boundary conditions have any significant effects on the results. The results are compared with the published literature to find the optimum configurations from the selected cases.

Table 1. The computational domain sizes and boundary conditions from numerical studies in the literature for flow over a circular cylinder at $Re = 3900$.

Study	Domain size	Lateral boundaries	Spanwise boundaries
Kravchenko and Moin (2000)	$30D$ radius and	-	-
Parnaudeau et al. (2008)	πD span length	-	Periodic
Lysenko, Ertesvåg, and Rian (2012)	$20D \times 20D \times \pi D$	Periodic	Periodic
Sidebottom, Ooi, and Jones (2015)	$25D$ radius and	-	-
Pereira et al. (2018)	πD span length	-	Periodic
	$24D \times 14D \times \pi D$	-	Periodic
	$50D \times 24D \times 3D$	Zero-gradient	Symmetry

Table 2. The flow parameters from published studies for flow over a circular cylinder at $Re = 3900$.

Study	St	$\langle L \rangle / D$	$- \langle u_{min} \rangle / U_\infty$
Urengo and Shih (1993) (experiment)	0.22	1.19	0.24
Parnaudeau et al. (2008) (experiment)	0.21	1.51	0.34
Parnaudeau et al. (2008) (LES)	0.21	1.56	0.26
Kravchenko and Moin (2000) (LES)	0.21	1.35	0.37
Lysenko, Ertesvåg, and Rian (2012) (LES)	0.19	0.90	0.26

2. Mathematical and numerical models

An in-house code has been developed in C++ based on the Finite Volume Method. This code is part of a longer term effort to simulate moving solid bodies in fluid flow applications, such as vortex-induced vibration. To model moving solid objects simply on a Cartesian grid, an immersed boundary method (IBM) of direct-forcing type is utilized, which will be explained in detail in Section 2.3. This method has already been used successfully in the past to simulate flows over multiple cylindrical objects (Chern, Hsu, and Horng 2012).

2.1. Governing equations and models

The non-dimensionalized continuity and Navier-Stokes equations for an incompressible Newtonian fluid are utilized for development of the code, which can be expressed as follows:

$$\nabla \cdot \mathbf{u} = 0, \quad (1)$$

$$\frac{\mathbf{u}}{t^*} + \nabla \cdot (\mathbf{u}\mathbf{u}) = -\nabla p + \frac{1}{Re} \nabla^2 \mathbf{u} + \mathbf{f}^*, \quad (2)$$

where \mathbf{u} , t^* , and p represent the fluid flow velocity, time and pressure, respectively. Reynolds number (Re) is given by $U_\infty D / \nu$, where U_∞ is the inlet velocity, D is the cylinder diameter and ν is the kinematic viscosity of the fluid. \mathbf{f}^* represents a virtual force applicable to the solid object only, to account for the direct-forcing.

The governing equations are discretized using the quadratic upstream interpolation for convective kinematics (QUICK) scheme (Leonard 1979). The present work uses a staggered grid to represent the velocities at the faces of the main cell. The temporal term is evaluated using third-order Adams-Bashforth scheme. Projection method is used to find the first intermediate velocity using:

$$\mathbf{u}^* = \mathbf{u}^m + \Delta t \left(\frac{1}{Re} \cdot \nabla^2 \mathbf{u} - \nabla \mathbf{u}\mathbf{u} \right)^m. \quad (3)$$

Next, the pressure Poisson equation can be solved in tandem with the continuity Equation (1) to determine the second intermediate velocity, \mathbf{u}^{**} ,

$$\mathbf{u}^{**} = \mathbf{u}^* - \nabla p^{m+1/2} \Delta t. \quad (4)$$

Bi-Conjugate Gradient Stabilized (Bi-CGSTAB) method is used to solve the pressure Poisson equation. Using the second intermediate velocity (\mathbf{u}^{**}) and the volume of solid function, η (calculation of η is described in Section 2.3), the final corrected velocity can be calculated by solving for the virtual force (\mathbf{f}^*),

Table 3. The different cases investigated in the present study, differentiated by their domain sizes and boundary conditions at the lateral and spanwise boundaries. All cases had the same inlet (Dirichlet with fixed velocity) and outlet (zero-gradient velocity) boundary conditions.

Case	Domain size	Lateral boundaries	Spanwise boundaries
Case 1	$16D \times 12D \times 3D$	Zero-gradient	Zero-gradient
Case 2	$16D \times 12D \times 3D$	Symmetry	Periodic
Case 3	$16D \times 12D \times 3D$	Periodic	Periodic
Case 4	$24D \times 14D \times 4D$	Zero-gradient	Zero-gradient
Case 5	$24D \times 14D \times 4D$	Symmetry	Periodic
Case 6	$24D \times 14D \times 4D$	Periodic	Periodic

$$\mathbf{f}^* = \eta \frac{\mathbf{u}_s^{m+1} - \mathbf{u}^{**}}{\Delta t}, \quad (5)$$

with

$$\mathbf{u}^{m+1} = \eta \mathbf{u}_s^{m+1} + (1 - \eta) \mathbf{u}^{**}, \quad (6)$$

where \mathbf{u}^{m+1} represents solid motion velocities, which are zero for the present case because the cylinder is stationary in all cases.

Smagorinsky model (Smagorinsky 1963) is used in the present study to model the small subgrid scales with a constant $C_s = 0.1$. The value of C_s used in past studies is typically between 0.1 and 0.2, based on the application. No wall model was selected for any specific near-wall treatment. This approach for turbulent flow over a cylinder is in agreement with the findings of Sidebottom, Ooi, and Jones (2015) who conducted a parametric study and noted that there were only small differences in the results from Smagorinsky model and the one-equation eddy viscosity model. Although they found that the use of a wall model to improve accuracy in the simulation of near-wall flow had a significant impact on the results not only near the wall but also several diameters downstream of the cylinder, the wall model only improved the results for some characteristics while worsening the results for others. Therefore, no conclusive benefit was observed from the use of a wall model and hence, the present study does not employ any.

2.2. Boundary conditions

The boundary conditions used for the different cases in the present work are briefly introduced here, mathematically. More details can be found in Versteeg and Malalasekera (2007). For all cases, a constant-velocity boundary condition (Dirichlet) is applied at the inflow with the spanwise and transverse velocity components set to zero and the streamwise velocity given a uniform flow profile, i.e.:

$$\mathbf{u} = U_\infty, v = w = 0. \quad (7)$$

At the outflow boundary in all cases, zero-gradient boundary conditions (Neumann) are applied for all the velocity components, i.e.:

$$\frac{\partial \mathbf{u}}{\partial x} = \frac{\partial v}{\partial x} = \frac{\partial w}{\partial x} = 0. \quad (8)$$

Zero-gradient pressure conditions are applied to all the boundaries in all cases, except the periodic boundaries. This implies:

$$\frac{\partial p}{\partial n} = 0, \quad (9)$$

where n signifies the direction normal to the boundary.

For cases where a symmetry boundary condition is used for the lateral boundary, symmetry plane conditions are applied as:

$$\frac{\partial \mathbf{u}}{\partial y} = \frac{\partial w}{\partial y} = v = 0. \quad (10)$$

In cases where a periodic boundary condition is used, all the variables are given values from the second last cell on the

opposite side of the computational domain. For example, in the z-direction:

$$\phi_{i,j,0} = \phi_{i,j,n_z-1} \text{ and } \phi_{i,j,n_z} = \phi_{i,j,1}, \quad (11)$$

where ϕ represents any variable, subscripts i and j represent the indexes in the x - and y -directions, and subscript n_z represents the index of the last cell in the z -direction (the spanwise direction assumed in this study). For the velocity component in the axis direction of the boundary considered (w velocity for the example of z -direction axis given above), a slightly different indexing is necessary to account for the staggered grid selected in the current work. Moreover, no-slip boundary condition is assumed at the cylinder surface. The choice of the set of boundary conditions for various cases is described in Section 2.4.

2.3. Direct-forcing immersed boundary method

The present work uses direct-forcing immersed boundary (DFIB) method to model the interactions between fluids and solids. The approach discussed below has been successfully used in earlier works for various problems involving the circular cylinder (Chern et al. 2014, 2015, 2018).

A variable η is used to distinguish between the cells occupied by fluid and solid in the computational domain, which represents the volume of solid (VOS). A value of $\eta = 1$ indicates a cell completely occupied by the solid, whereas $\eta = 0$ represents a cell completely occupied by the fluid. Figure 1 represents the details of this concept where Figure 1(a) describes the steps of the algorithm for determining η and Figure 1(b) shows the representation of η on the computational domain.

The present work utilizes a subgrid method to further refine the calculation of η to determine a precise solid boundary, without the need to use a finer computational grid. This method can be described with respect to Figure 1(a,c)

From Figure 1, $D_{m,n}$ is the distance measured from the cylinder center to the computational grid cell center (ignoring the spanwise direction). When $D_{m,n}$ is greater than the cylinder radius, R , the VOS is zero and vice versa. However, when the difference between $D_{m,n}$ and R is less than half the diagonal of a cell, then, the cell could lie at the boundary between the solid and the fluid. This is where subgrid method should be applied.

In the subgrid method, the cell is divided further into subgrids (50 subgrids are used in the present study) and the same algorithm earlier used for $D_{m,n}$ is now used for $d_{i,j}$, which is the distance measured from the cylinder center to the subgrid center. If $d_{i,j}$ is larger than R , then another variable representing VOS of the subgrid cell, $\xi = 0$ but if $d_{i,j}$ is smaller than R , then $\xi = 1$. For every grid cell where the subgrid method is applied, the average of all the subgrid cell VOS (ξ) is determined, which is equated to the overall cell VOS, η . Figure 2 shows the refined cylinder profile that can be achieved using the subgrid method without any modification of the main computational grid.

2.4. Details of the cases and other numerical information

In this section, we discuss the choice of the computational domain sizes and the boundary conditions, the selection of

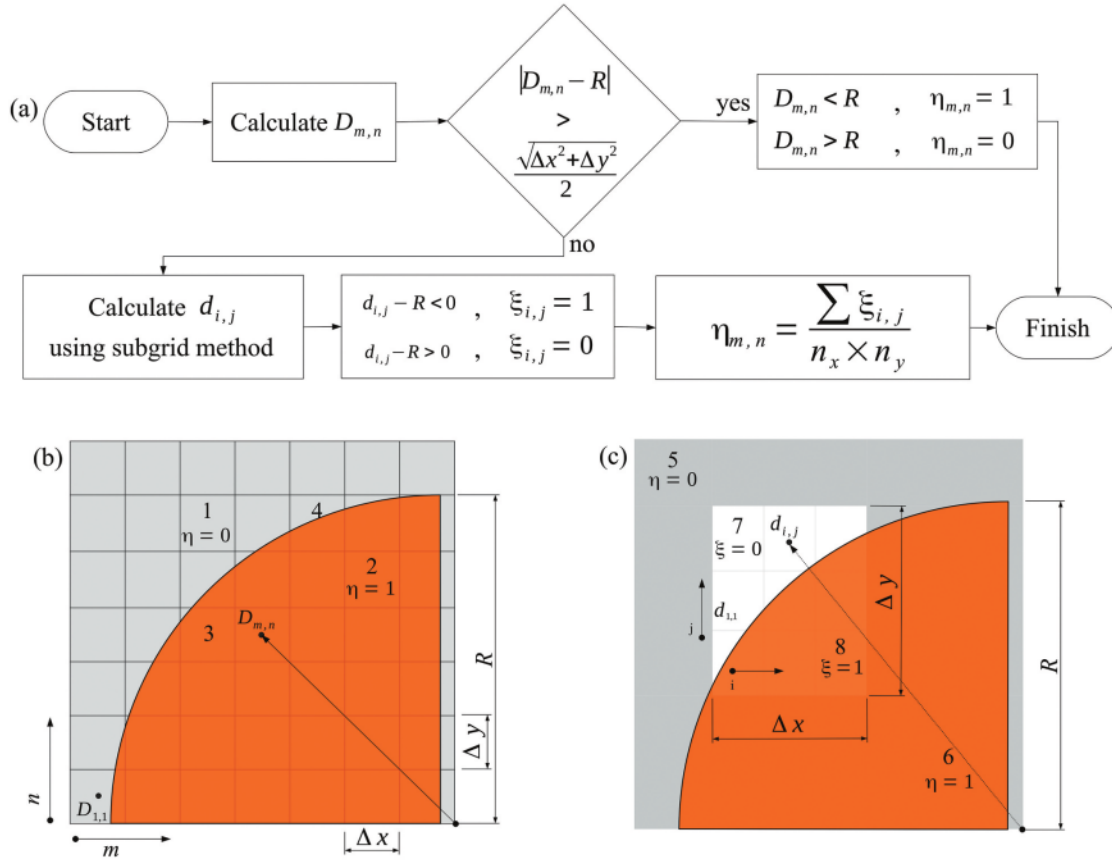


Figure 1. Description of the subgrid method and the algorithm to determine η ; (a) flow chart describing the steps in calculation of volume of solid (VOS); (b) illustration of grid cells to define η ; (c) illustration of subgrid cells to define ξ .

the grid sizes and the grid independence test. Finally, the computer hardware used for the present study is described.

The computational domain for the present work is presented in Figure 3 with the labeled distances listed in Table 4. Two different sizes of computational domains were selected for comparison and each of them was tested with three sets of boundary conditions, as stated in Table 3.

Tezduyar and Shih (1991) carried out 2-D numerical experiments for flow over a cylinder to find that the downstream boundary could be fixed $14.5D$ away from the cylinder. They also found that even when the downstream boundary is brought closer to the cylinder up to only $6.5D$ away from the cylinder, the effect on the results is very minor. Although their analysis was conducted for $Re = 100$, other researchers have also adopted similar downstream distances for different Reynolds numbers. Labbé and Wilson (2007) used $15D$ for comparing over a range of Re from 100 to 1000. For $Re = 3900$, Parnaudeau et al. (2008) used $15D$ and Sidebottom, Ooi, and Jones (2015) used $17D$ for the downstream distance. Therefore, we have opted to use 17.5 for the large domain cases. For the small domain, we selected a downstream distance of $9.5D$, which is still greater than the $6.5D$ distance suggested by Tezduyar and Shih (1991) that caused only minor changes in results at $Re = 100$.

Past numerical studies at $Re = 3900$ for cuboid computational domains have been conducted with upstream distances of $5D$ (Parnaudeau et al. 2008), $7D$ (Sidebottom, Ooi, and Jones 2015) and $10D$ (Pereira et al. 2018). Both cases in this study have used an upstream distance of $6.5D$. Therefore, any difference in the results is not due to the influence of the upstream distance, which has not been investigated further.

The selected lateral distance for the cuboid computational domains varies widely in the literature. Pereira et al. (2018) used $24D$, Parnaudeau et al. (2008) used $20D$, whereas Sidebottom, Ooi, and Jones (2015) used $14D$ as the lateral length of the cuboid domain. In this work, a lateral distance of $14D$ has been selected for the large domain and $12D$ for the smaller domain to investigate its influence.

The most popular choice for the spanwise domain length in the numerical studies conducted at $Re = 3900$ is πD , which was used by Kravchenko and Moin (2000); Parnaudeau et al. (2008); Lysenko, Ertesvåg, and Rian (2012); Sidebottom, Ooi, and Jones (2015), although Pereira et al. (2018) used $3D$. Therefore, a spanwise distance of $3D$ has been chosen for the smaller domain and $4D$ for the larger domain to incorporate the effect of both of these choices while ensuring that the larger domain

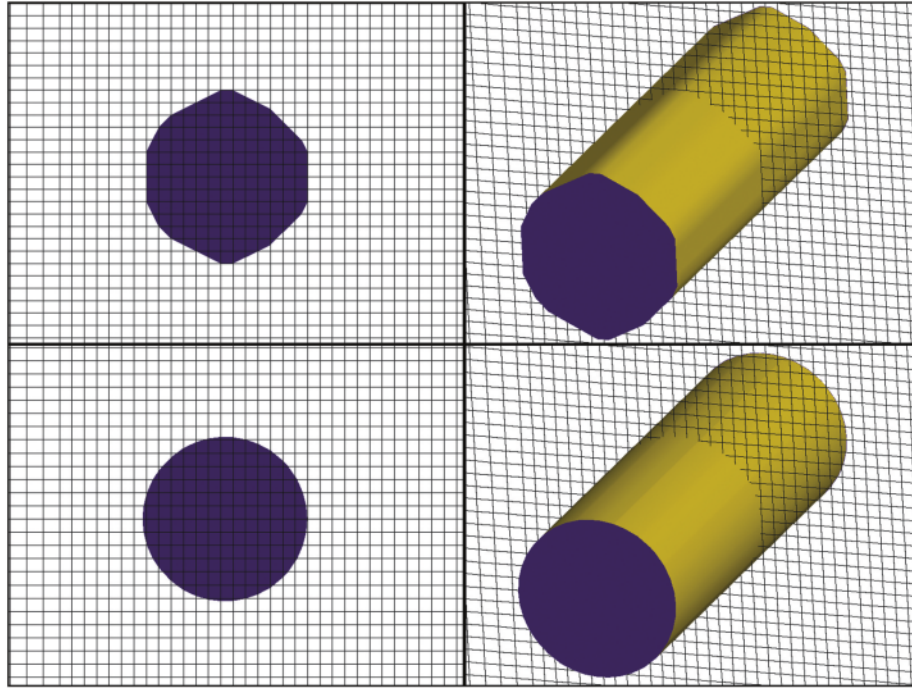


Figure 2. Comparison of the cylinder profiles without sub-grid method (top) and with sub-grid method (bottom).

Table 4. Values of the distances shown in Figures 3 and Figures 4 for the two sets of computational domain sizes used in this study.

Distance	Small domain cases 1, 2, and 3	Large domain cases 4, 5, and 6
x_1	$6.5D$	$6.5D$
x_2	$9.5D$	$17.5D$
y_1	$6D$	$7D$
y_2	$6D$	$7D$
z_1	$3D$	$4D$
x_s	$3D$	$3D$
x_{f1}	$5.5D$	$5.5D$
x_{f2}	$7.5D$	$15.5D$
y_s	$4D$	$4D$
y_{f1}	$4D$	$5D$
y_{f2}	$4D$	$5D$

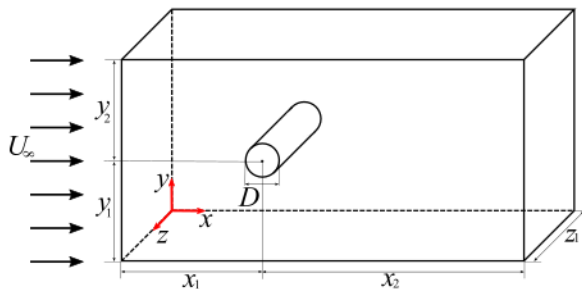


Figure 3. Computational domain in the present study. The flow is in x -direction (streamwise), y -axis is the lateral (transverse) direction and the cylinder axis (spanwise) is in z -direction. Values of the distances are listed in Table 4 for each of the two domain sizes.

exceeds the commonly used value to minimize any non-physical effects it may have on the results.

For each domain size, three sets of boundary conditions have been tested. The inlet and outlet boundary conditions are the same for all cases, as described in Section 2.2. Based on the precedent of Lei, Cheng, and Kavanagh (2001) and Labbé and Wilson (2007), a symmetry boundary condition for the lateral boundaries and a periodic boundary condition for the spanwise boundaries was selected for a set. Another set of boundary conditions was based on the choice of Parnaudeau et al. (2008) who adopted periodic boundary conditions at both the lateral and spanwise boundaries. A simple zero-gradient boundary at the lateral and the spanwise boundaries was chosen as the third set for comparison.

For all of the cases, a finer grid was applied around the cylinder and immediately behind the cylinder, as shown in Figure 4 with the relevant distances listed in Table 4. $y^+ = 20$ was selected because Sidebottom, Ooi, and Jones (2015) found that the accuracy was affected at $y^+ > \sim 30$. For the coarser grid away from the cylinder in x - and y -directions as well as the z -direction (uniform grid is used in z -direction), grid independence tests were conducted for each of the domain sizes by varying the number of cells. The results of the grid independence test are presented for both domain sizes in Tables 5 and 6. Based on these results, the number of grids listed as ‘medium’ were selected for each of the domains due to the relatively small variation in the value of $\langle u_{\min} \rangle$ for each case when the number of grids is increased to the ‘fine’ level.

As discussed, this study was conducted using an in-house solver developed in C++. The solver was parallelized using

Table 5. Grid independence test results for the small domain.

Grid	Number of grids	$-\langle u_{\min} \rangle / U_{\infty}$
Coarse	135,000	0.154
Medium	884,000	0.241
Fine	1,330,000	0.273

Table 6. Grid independence test results for the large domain.

Grid	Number of grids	$-\langle u_{\min} \rangle / U_{\infty}$
Coarse	270,000	0.225
Medium	1,500,000	0.223
Fine	2,240,000	0.223

OpenMP. The numerical simulations were executed on a cluster consisting of Dell T630 workstations, each having 20 cores of the type Intel Xeon CPU E5-2650v3 (2.30 GHz).

3. Results and discussion

All the results in the present work have been averaged over a large number of timesteps (except where stated explicitly). Franke and Frank (2002) investigated flow over a circular cylinder at $Re = 3900$ using a finite volume code for the compressible Navier-Stokes equations and recommended averaging times longer than $tU_{\infty}/D = 200$. Therefore, in this work, averaging for the results starts from $tU_{\infty}/D = 300$ to 600 for all the cases (including the grid independence tests). Since simple uniform initial conditions throughout the computational domain were used, the results earlier than $tU_{\infty}/D = 300$ were ignored to avoid the initial perturbations.

3.1. Strouhal number and recirculation region characteristics

The recirculation region characteristics have been averaged over time, as described above, as well as in the z -direction. Table 7 compares the Strouhal number (St), the normalized mean recirculation length ($\langle L_r \rangle / D$) and the normalized minimum mean streamwise velocity ($-\langle u_{\min} \rangle / U_{\infty}$) at the centerline for the various cases in the present study with published literature.

In this work, the Strouhal number has been evaluated using Fast Fourier Transform (FFT) of the v -velocity component at $1.06D$ downstream of the cylinder in the center of y - and z -planes. The St number matches the earlier experimental and numerical studies for all of the cases. This shows that even the smaller domain correctly captures the frequency of vortex shedding and the different sets of boundary conditions tested do not have much effect on the St number.

For the small domain cases, $\langle L_r \rangle$ and $-\langle u_{\min} \rangle$ are generally within the range of published results, though $\langle L_r \rangle$ for case 2 is slightly larger than 1.56, which was reported by Parnaudeau et al. (2008). The recirculation length occurs immediately downstream of the cylinder and $-\langle u_{\min} \rangle$ also occurs only in the recirculation region. Since the small domain encompasses this region completely, its ability to correctly predict such flow characteristics of the recirculation region is possible. Symmetry boundary condition on the lateral boundaries (case 2) appears to increase $\langle L_r \rangle$ whereas periodic boundary

condition on the lateral boundaries (case 3) gives a smaller value of $\langle u_{\min} \rangle$ for the smaller domains, though still within the range observed in published results.

Analyzing the results for the larger domain cases, only case 5 with symmetry condition on the lateral boundaries and periodic condition on the spanwise boundaries can approach the published results for both $\langle L_r \rangle$ and $\langle u_{\min} \rangle$, though $\langle u_{\min} \rangle$ is slightly higher. This suggests that perhaps the correct selection of boundary conditions is even more important when the computational domain size is larger.

3.1.1. Velocity fluctuations

The time histories of individual components u , v and w for every case throughout the simulation at $1.06D$ downstream of the cylinder in the center of y - and z -planes is shown in Figure 5. Case 1 using a small domain size with zero-gradient lateral and spanwise boundaries fails to maintain three-dimensional turbulence throughout the simulation as the w -velocity fluctuations reduce to almost zero after the initial perturbations and the v -velocity fluctuations become quite large. This could mean that the zero-gradient boundary conditions are not adequate for accurately simulating turbulent flow for the smaller domain size. Also, for the smaller domain, periodic boundary conditions on both lateral and spanwise sides in case 3 lead to higher v -velocity fluctuations than case 2, where symmetry boundary condition is set on the lateral sides.

Case 4 with zero-gradient boundary conditions for the larger domain shows velocity fluctuations quite different from case 1, which had the same boundary conditions but with a smaller domain size. The velocity fluctuations in case 4 are similar to those displayed in case 1 for the duration of $tU_{\infty}/D = 120 - 180$, before the w -velocity component flattened. Cases 5 and 6 display results similar to their counterpart cases 2 and 3 for the smaller domain, though the v -velocity fluctuations are slightly smaller in case 6 than case 3.

The frequency of the transverse velocities calculated using Fast Fourier Transform (FFT) at $1.06D$ downstream of the cylinder in the center of y - and z -planes is shown in Figure 6. It should be noted that some of the turbulence displayed by these frequencies may not be real and could be induced due to the effect of the smaller domain size or the boundary conditions, which have caused non-physical Reynolds stresses. The proper domain size and boundary conditions should not induce redundant fluctuations. From Figure 6, we notice that case 1 displays several peaks other than the highest one. The least fluctuations can be observed for the cases 2 and 5 with periodic boundary conditions on the spanwise boundaries and symmetry boundary conditions on the lateral boundaries.

3.1.2. Mean streamwise velocities

The mean streamwise velocities at the horizontal centerline in the wake of the cylinder for the small and large domain cases is shown in Figure 7. A quick comparison of the present results for the small and large domain sizes shows that the smaller domain cases are generally more accurate in the near wake region of the cylinder including the recirculation region, but show non-physical oscillations after three diameters downstream of the cylinder.

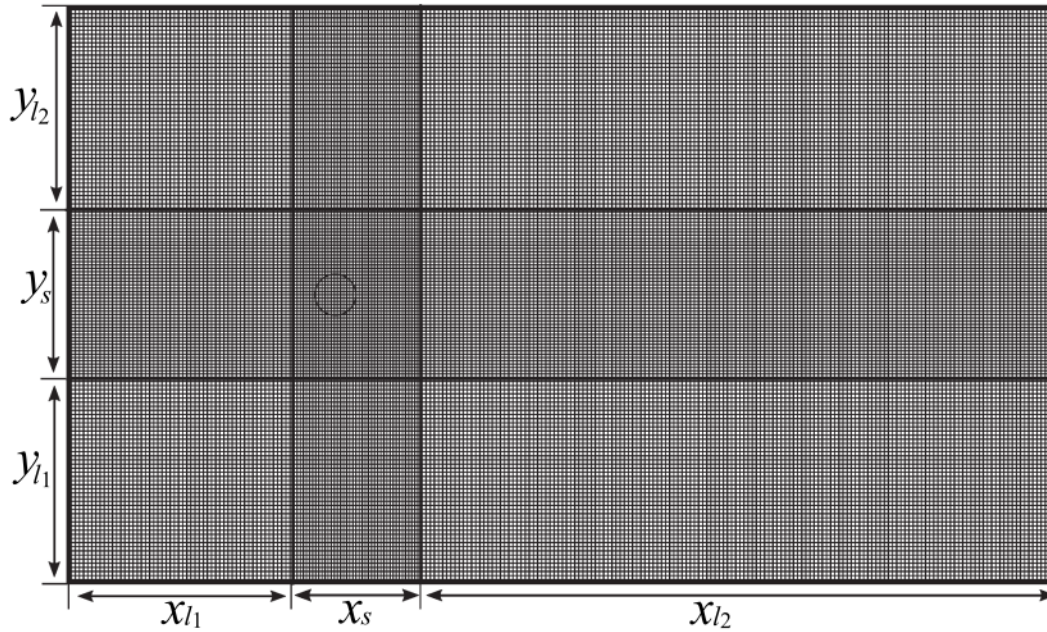


Figure 4. A side-view of the grid chosen for the present study. A finer grid is selected around the cylinder (represented by the distances x_s and y_s) and a coarser grid is adopted for areas away from the cylinder. In the z -direction, the grid is uniform. Values of all the distances are listed in Table 4 for each of the two domain sizes.

Table 7. Comparison of the Strouhal number (St), the normalized mean recirculation length ($\langle L_r \rangle / D$) and the normalized minimum mean streamwise velocity ($-\langle u_{\min} \rangle / U_{\infty}$) for various cases in the present study.

Case	St	$\langle L_r \rangle / D$	$-\langle u_{\min} \rangle / U_{\infty}$
Published studies	0.19–0.22	0.9–1.56	0.24–0.37
Case 1 (small domain)	0.194	1.247	0.244
Case 2 (small domain)	0.205	1.662	0.241
Case 3 (small domain)	0.197	1.258	0.343
Case 4 (large domain)	0.208	0.817	0.129
Case 5 (large domain)	0.197	1.562	0.223
Case 6 (large domain)	0.209	1.042	0.199

For the smaller domain, cases 1 and 3 have lesser accuracy in the near wake as the position of their $\langle u_{\min} \rangle$ does not coincide with the previous studies. Case 1 results lie closer to the published results of Lourenco and Shih (1993) in the near wake, but in the far wake region it displays widely oscillatory behavior. Such oscillations of velocities in the far wake are also present for the other two smaller domain cases but to a much lesser extent. The most accurate among the smaller domain cases is case 2 with a combination of periodic and symmetry boundary conditions. Case 2 results in the near wake coincide with the published experimental and numerical results of Parnaudeau et al. (2008). However, in the far wake, the accuracy diminishes.

Another noticeable phenomenon is the gradual reversal of velocity downstream of the cylinder in cases 2 and 5, which also occurs in the results of Parnaudeau et al. (2008). This is observed as a slightly flatter curve which starts behind the cylinder in this case, as compared to the immediate decline of the velocity in the other cases. Along with this, the location of the minimum velocity $\langle u_{\min} \rangle$ is also different in each case of

results. This observation indicates the importance of the lateral boundaries because the only difference of cases 2 and 5 from cases 3 and 6 is that the first two have symmetry boundary condition on the lateral boundaries whereas the latter two have periodic boundary condition on the lateral boundaries. But the effect they have on velocity downstream of the cylinder is distinct, especially in the near wake.

For the large domain cases, the most obvious difference is the marked improvement in the results of the far wake region with the absence of any oscillations of velocity. Case 5 with a combination of periodic and symmetry boundary conditions provides the best results that are quite close to the numerical results of Parnaudeau et al. (2008) throughout the horizontal centerline. Therefore, this suggests that the effect of the computational domain size is more pronounced on the far wake region. For the near wake region among the larger domain cases, case 6 approaches the experimental results of Lourenco and Shih (1993) and case 5 approaches the numerical results of Parnaudeau et al. (2008). This will be discussed further with respect to the transverse variation of the mean streamwise velocity in the next section.

Comparing between the small and large domain cases using Figure 8(a), it can be seen that the smaller domain cases generally have a lower $\langle u_{\min} \rangle$ in the near wake and a non-physical oscillatory behavior in the far wake. However, the results for cases with periodic boundary condition on the spanwise boundaries and symmetry boundary condition on the lateral boundaries are very close to each other, regardless of the domain size. In fact, in the near wake region, the smaller domain size is able to provide results closer to the numerical results of Parnaudeau et al. (2008) than the larger domain size. This strongly suggests that the

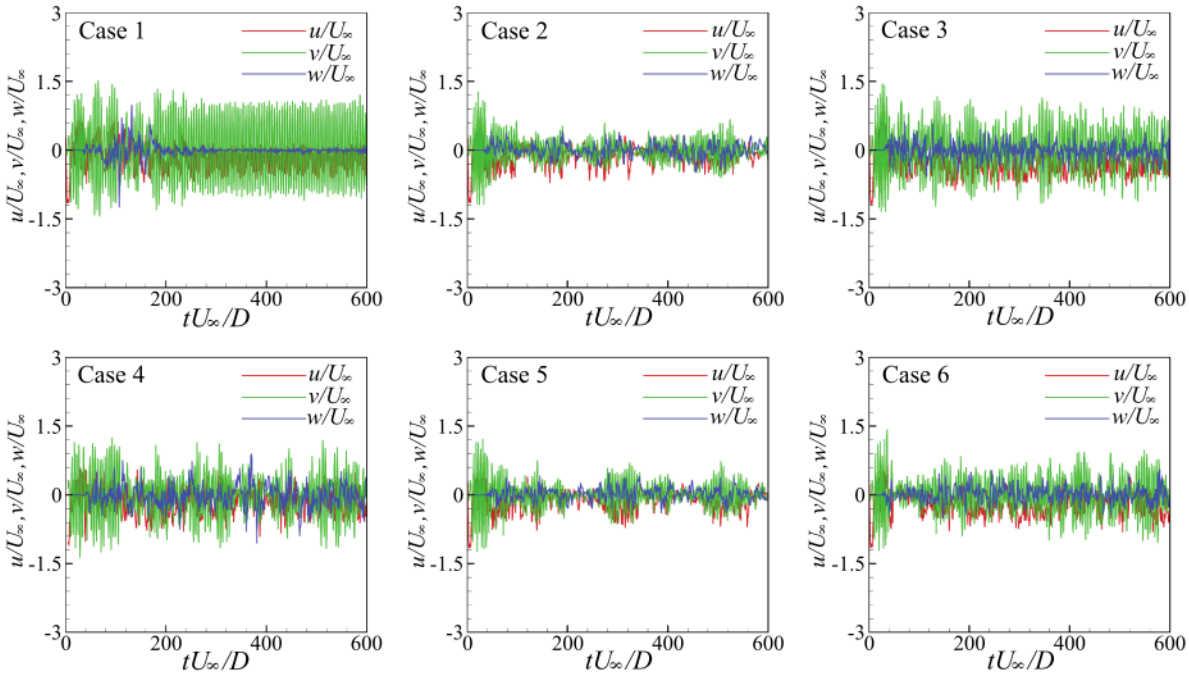


Figure 5. Time histories of the velocity components u , v and w for each case over the duration of simulation, $tU_\infty/D = 600$, at $1.06D$ downstream of the cylinder in the center of y - and z -planes.

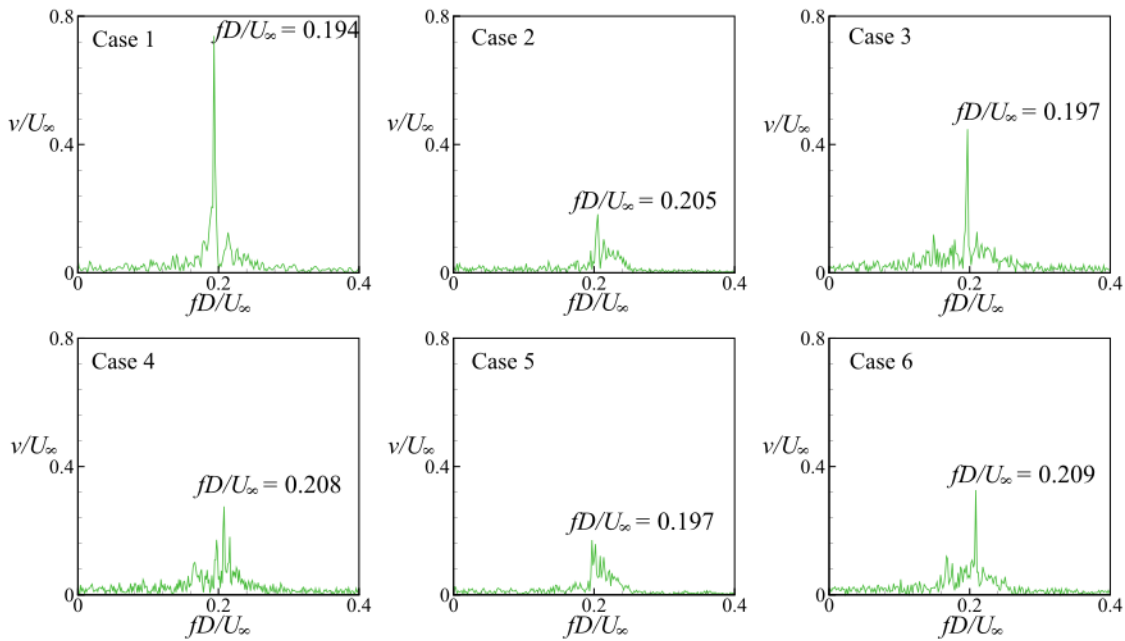


Figure 6. Transverse velocity frequencies determined using Fast Fourier Transform (FFT) for the v -velocity component for each case at $1.06D$ downstream of the cylinder in the center of y - and z -planes.

combination of symmetry and periodic boundary conditions on the lateral and spanwise boundaries, respectively, generates better results for this problem that are more likely to be independent of the domain size.

The mean streamwise velocities at a distance of $1.06D$ on a central 3D transverse line downstream of the cylinder are shown in Figure 9. The u -velocity curve behind the cylinder can be seen to have two distinct shapes in the published

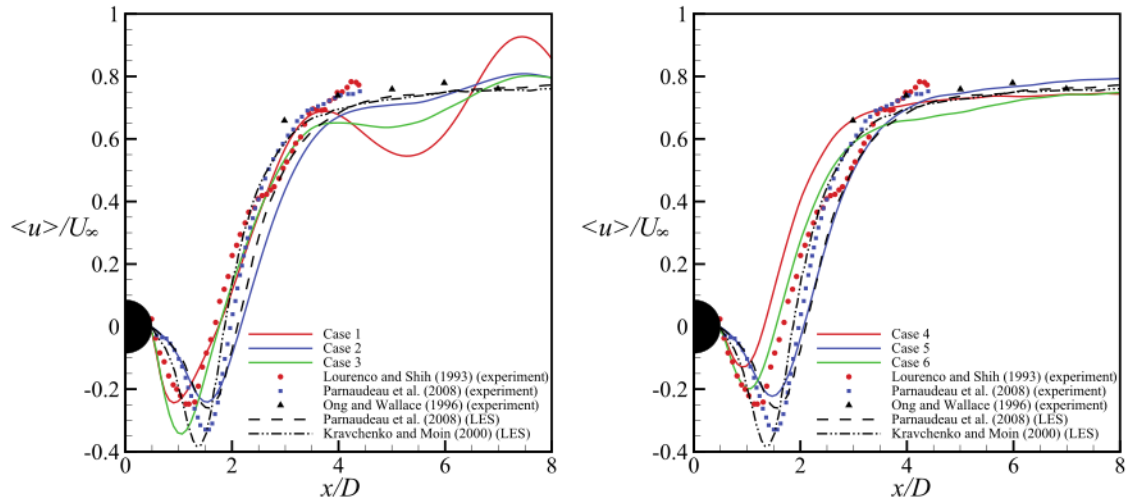


Figure 7. Mean streamwise velocities at the horizontal centerline in the wake of the cylinder for the small and large domain cases, compared with published literature.

literature. The experimental results of Lourenco and Shih (1993) have a V-shaped curve while the experimental and numerical results from Parnaudeau et al. (2008) have a U-shaped curve. Kravchenko and Moin (2000) have discussed the V-shaped results of Lourenco and Shih (1993) and attributed their V-shaped velocity profile to some external influences on their experimental setup that caused an earlier transition to turbulence.

It is interesting to note that the cases 2 and 5, with periodic boundary condition on the front and back and symmetry boundary condition on the top and bottom, have a distinctly U-shaped curve, while the other cases have a V-shaped profile. This indicates that the symmetry boundary condition at the top and bottom of the computational domain are important in

ensuring a U-shaped curve because cases 2 and 5 only differ from the cases 3 and 6 due to the lateral boundaries having symmetry boundary condition in the former case but periodic boundary condition in the latter case. Case 5 approaches the results of Parnaudeau et al. (2008) while case 6 shows good agreement with the experimental results of Lourenco and Shih (1993). A similar trend was also observed for the variation of mean streamwise velocities in the streamwise direction.

Switching the boundary condition at the lateral boundaries from periodic to symmetry condition can cause the u -velocity profile to approach the results of Lourenco and Shih (1993) in the former case and Parnaudeau et al. (2008) in the latter case. This behavior offers a possible explanation for the deviating results of Lourenco and Shih (1993). Any factor that influences

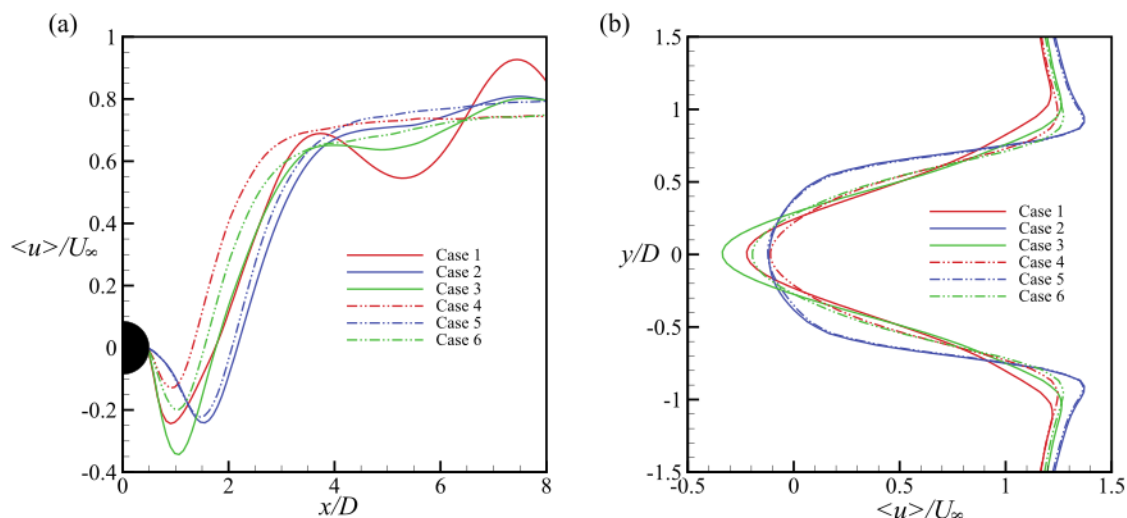


Figure 8. Comparison between the small and large domain cases for mean streamwise velocities (a) at the horizontal centerline in the wake of the cylinder; (b) at $x/D = 1.06$ downstream of the cylinder on a 3D transverse line.

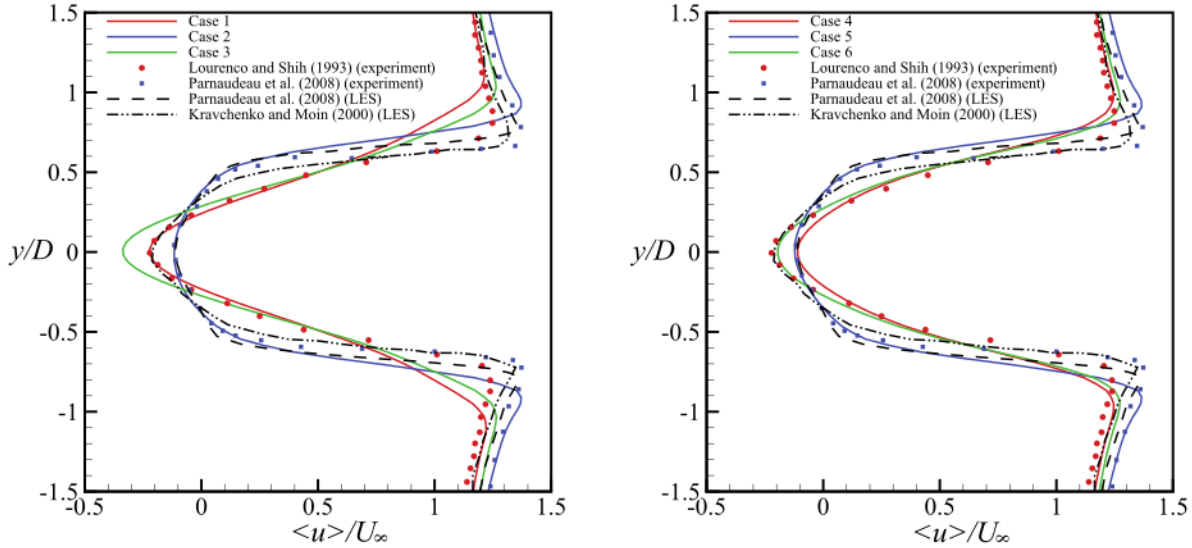


Figure 9. Mean streamwise velocities at $x/D = 1.06$ downstream of the cylinder on a 3D transverse line for the small and large domain cases, compared with published literature.

the flow to transition to turbulence quickly can transform the velocity profile at this location to a V-shape from a U-shape. In the case of the present numerical analysis, this can be attributed to the boundary condition at the lateral boundaries. For the experiment of Lourenco and Shih (1993), it may have been due to the physical features and the distance of the lateral boundaries in the experimental setup.

A comparison of the mean streamwise velocity variation in the transverse direction between the cases of this study, presented in Figure 8(b), shows that minimal changes are observed between case 2 for the small domain and case 5 for the large domain, both having the same boundary conditions. Other boundary conditions lead to noticeable differences when the domain size is changed. This proves that periodic boundary condition on the spanwise boundaries and symmetry boundary condition on the lateral boundaries minimize the effects of the domain size in the transverse direction as well as streamwise direction, as was observed for Figure 8(a).

Figure 10 shows a comparison of the large domain cases 4, 5 and 6 with the published results of Ong and Wallace (1996) and Kravchenko and Moin (2000). Case 5 for the larger domain with periodic spanwise boundary conditions and symmetric lateral boundary conditions is able to approach the experimental results of Ong and Wallace (1996) very closely, with better agreement than the results of Kravchenko and Moin (2000). This proves the earlier observation in Section 3.1 that among the cases tested in the present work, case 5 shows the most promising results.

3.1.3. Velocity and vorticity contours

Cases 2 and 5 with the same boundary conditions have shown good results for both the domain sizes. Their various flow features are further examined in this section. The instantaneous contours of $u -$, $v -$ and $w -$ velocity components in the mid-

y planes for cases 2 and 5 for ten diameters downstream of the cylinder are shown in Figure 11. These results could be compared with similar results shown by Kravchenko and Moin (2000) (Figures 2, Figures 3, and Figures 4). The unsteady recirculation region can be clearly observed for the u -velocity components in both figures, though the unsteadiness is more distinguishable for the larger domain. The alternating regions of positive and negative cross-flow (v) velocity components indicating the vortical structures can also be observed in both figures. Different sizes of vortical structures are present and the

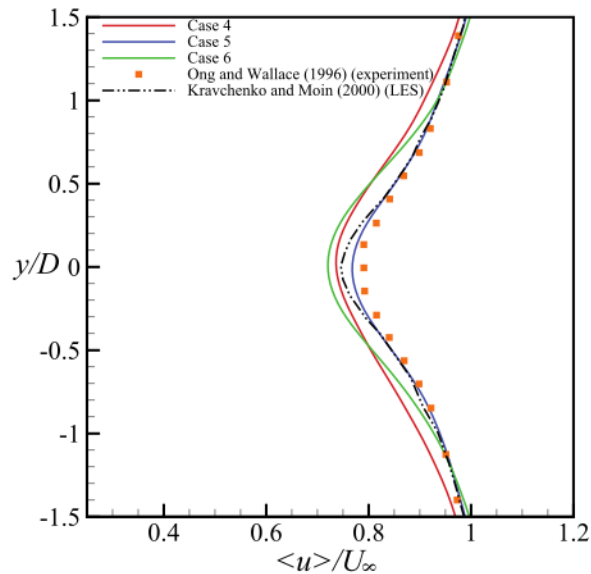


Figure 10. Mean streamwise velocities at $x/D = 6.0$ downstream of the cylinder on a 3D transverse line, compared with published literature.

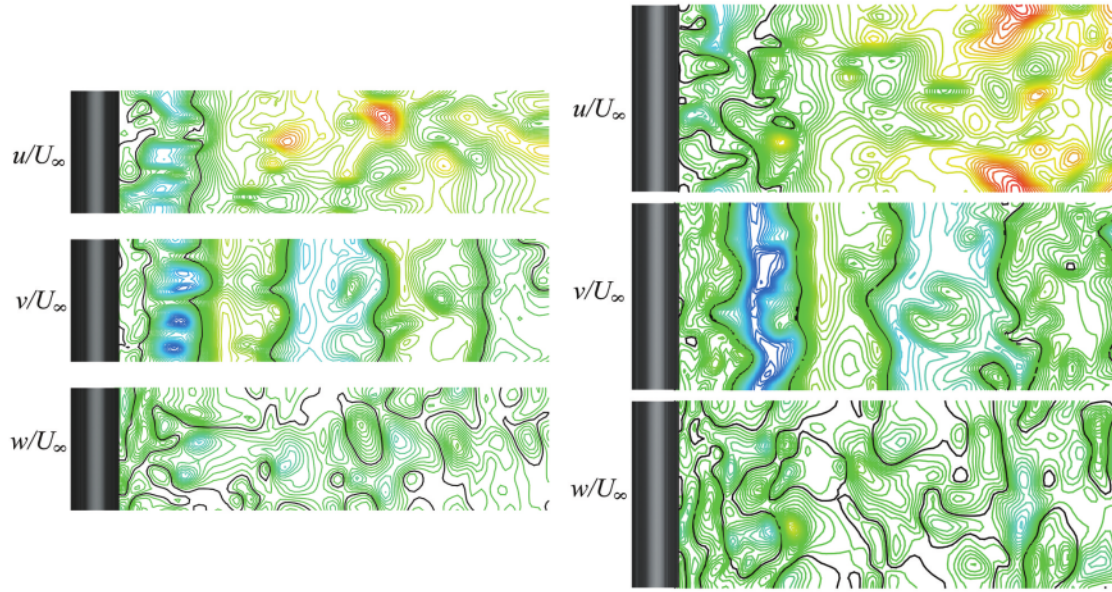


Figure 11. Top-views of instantaneous contours of u -, v - and w - velocities for flow over the cylinder in the xz -plane at the center of the y -axis for the first ten diameters downstream of the cylinder, for the small-domain case 2 (left) and large-domain case 5 (right). There are 60 contours levels from -1.3 to 1.7 and the solid black lines represent the contours with zero-velocity.

wake is fully three-dimensional and turbulent. The distance between the negative and positive alternating velocities increases in the downstream direction and so does the general size of the flow structures. But some small scale flow structures are also present in the downstream part of the flow, as shown by the spanwise velocity contours. These observations are in close agreement with the results presented by Kravchenko and Moin (2000).

Figure 12 shows a comparison of the $\langle u \rangle$ -velocity contours around the cylinder for case 2 and case 5, which can be compared with the published results of Pereira et al. (2018, Figure 7) for modeled turbulence kinetic energy fraction, $f_k = 0.15$, and Parnaudeau et al. (2008, Figure 16). Both cases agree well with each other as well as with the earlier published results. This proves that using symmetry boundary condition on the lateral boundaries and periodic boundary condition on the spanwise boundaries, both computational domain sizes can adequately resolve the u -velocity components in the immediate vicinity of the cylinder and the near wake region.

Figure 13 shows a final comparison of the flow structures for small and large domains, visualized using Q-criterion (Hunt, Wray, and Moin 1988) with vorticity magnitudes represented by colored contours. In both cases, the laminar boundary layer separation followed by a completely turbulent wake can be clearly observed, which is typical of the subcritical flow regime around a circular cylinder at $Re = 3900$.

4. Conclusions

The effect of computational domain size and boundary conditions on flow over a circular cylinder at $Re = 3900$ was investigated. Two domain sizes and three different sets of boundary conditions

were tested. Strouhal number, the normalized mean recirculation length, the normalized minimum mean streamwise velocity, time histories of velocities, velocity fluctuations, mean velocity profiles in the streamwise and transverse directions and different velocity contours were used to compare the results with published literature. The capability of the adopted DFIB method in simulating fluid-structure interactions in turbulent flow was proven.

It was found that the domain size has a significant impact on the results, especially in the far wake region downstream of the cylinder. It was also noted that the effect of the domain size was particularly significant for some of the boundary conditions. However, periodic spanwise boundaries and symmetric lateral boundaries (cases 2 and 5) minimized the influence of the domain size, especially in the near wake region.

The boundary conditions were also found to exert a significant influence on the results with periodic boundary condition on the lateral and spanwise boundaries leading to a more V-shaped transverse u -velocity profile at $x/D = 1.06$. Whereas symmetry boundary condition on the lateral boundaries and periodic boundary conditions on the spanwise boundaries gave a U-shaped profile at the same location. Both sets of boundary conditions for the larger domain had good agreement with two different sets of published experimental results. Thus, it appears that the type of boundary condition at the lateral boundaries can also force an earlier transition of the flow to turbulence in the streamwise direction, leading to a V-shaped profile. This suggests that the long-standing issue of the contradiction in experimental results for velocity profiles at $x/D = 1.06$ for $Re = 3900$ (Kravchenko and Moin 2000; Parnaudeau et al. 2008) could possibly be caused by physical features and distances of the lateral sides of the experimental setup.

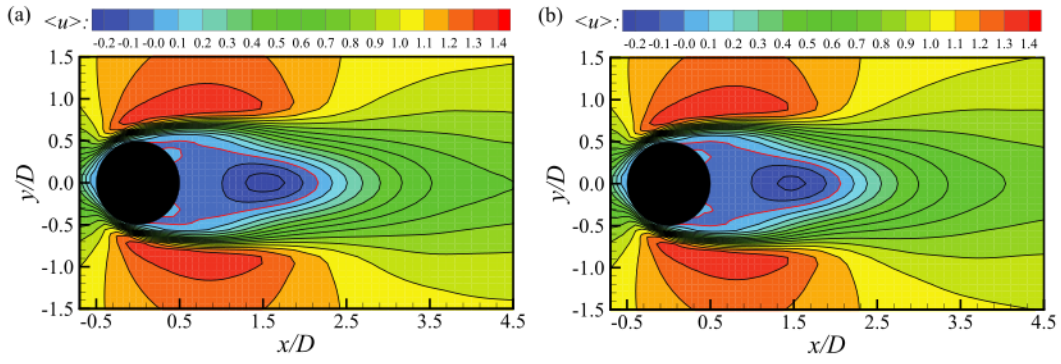


Figure 12. Side-view of average u -component velocity contours for flow over the cylinder for present study (a) case 2; (b) case 5. These results can be compared with Pereira et al. (2018, Figure 7) and Pamaudeau et al. (2008, Figure 16).

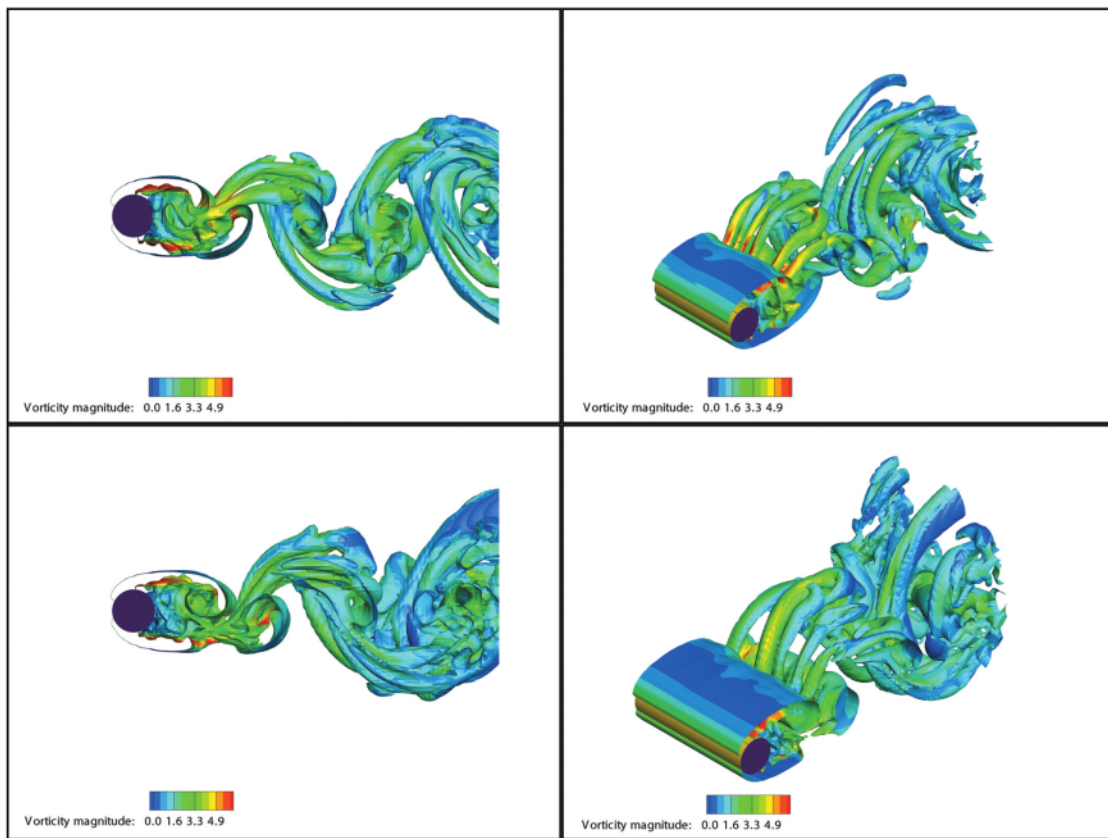


Figure 13. Instantaneous flow structures visualized using Q-criterion at value 0.01 for case 2 (top) and case 5 (bottom). The vorticity magnitude is represented using colored contours.

Overall, the larger domain with periodic spanwise boundary conditions and symmetric lateral boundary conditions provided the best results, though the smaller domain with the same boundary conditions was also able to predict several flow parameters accurately, especially in the near wake region next to the cylinder.

Disclosure Statement

No potential conflict of interest was reported by the author(s).

Funding

The authors express their gratitude for the financial support from Ministry of Science and Technology, Taiwan [grant no. MOST-107-2221-E-011-075-MY3].

ORCID

Syed Ahmad Raza  <http://orcid.org/0000-0003-2756-5020>

Yosua Heru Irawan  <http://orcid.org/0000-0001-9615-3447>

Ming-Jyh Chern  <http://orcid.org/0000-0002-7815-9455>

References

- Beaudan, P., and P. Moin. 1994. "Numerical Experiments on the Flow past a Circular Cylinder at Sub-Critical Reynolds Number." Technical Report No. TF-62. Stanford, CA, US: Department of Mechanical Engineering, Stanford University.
- Behr, M., D. Hastreiter, S. Mittal, and T. E. Tezduyar. 1995. "Incompressible Flow past a Circular Cylinder: Dependence of the Computed Flow Field on the Location of the Lateral Boundaries." *Computer Methods in Applied Mechanics and Engineering* 123 (1): 309–316. doi:10.1016/0045-7825(94)00736-7.
- Breuer, M. 1998. "Numerical and Modeling Influences on Large Eddy Simulations for the Flow past a Circular Cylinder." *International Journal of Heat and Fluid Flow* 19 (5): 512–521. doi:10.1016/S0142-727X(98)10015-2.
- Chern, M. -J., W. -C. Hsu, and T. -L. Homg. 2012. "Numerical Prediction of Hydrodynamic Loading on Circular Cylinder Array in Oscillatory Flow Using Direct-Forcing Immersed Boundary Method." *Journal of Applied Mathematics* 2012: 1–16. doi:10.1155/2012/505916.
- Chern, M. -J., Y. -H. Kuan, G. Nugroho, G. -T. Lu, and T. -L. Homg. 2014. "Direct-Forcing Immersed Boundary Modeling of Vortex-Induced Vibration of a Circular Cylinder." *Journal of Wind Engineering and Industrial Aerodynamics* 134: 109–121. doi:10.1016/j.jweia.2014.08.015.
- Chern, M. -J., G. T. Lu, Y. H. Kuan, S. Chakraborty, G. Nugroho, C. B. Liao, and T. -L. Homg. 2018. "Numerical Study of Vortex-Induced Vibration of Circular Cylinder Adjacent to Plane Boundary Using Direct-Forcing Immersed Boundary Method." *Journal of Mechanics* 34 (2): 177–191. doi:10.1017/jmech.2017.55.
- Chern, M. -J., D. Z. Noor, C. -B. Liao, and T. -L. Homg. 2015. "Direct-Forcing Immersed Boundary Method for Mixed Heat Transfer." *Communications in Computational Physics* 18 (4): 1072–1094. doi:10.4208/cicp.151214.250515.
- Franke, J., and W. Frank. 2002. "Large Eddy Simulation of the Flow past a Circular Cylinder at ReD=3900." *Journal of Wind Engineering and Industrial Aerodynamics* 90 (10): 1191–1206. doi:10.1016/S0167-6105(02)00232-5.
- Hunt, J. C. R., A. A. Wray, and P. Moin. 1988. "Eddies, Streams, and Convergence Zones in Turbulent Flows." In *Studying Turbulence Using Numerical Simulation Databases, 2. Proceedings of the 1988 Summer Program*, CA, US, 1 December 1988: 193–208. CA, US: Center for Turbulence Research, Stanford University.
- Jang, J. -Y., T. -L. Liu, K. -C. Pan, and T. -W. Chu. 2019. "Numerical Investigation on the Hydrodynamic Performance of Amphibious Wheeled Armored Vehicles." *Journal of the Chinese Institute of Engineers* 42 (8): 700–711. doi:10.1080/02533839.2019.1660225.
- Kravchenko, A. G., and P. Moin. 2000. "Numerical Studies of Flow over a Circular Cylinder at ReD=3900." *Physics of Fluids* 12 (2): 403–417. doi:10.1063/1.870318.
- Labbé, D. F. L., and P. A. Wilson. 2007. "A Numerical Investigation of the Effects of the Spanwise Length on the 3-D Wake of A Circular Cylinder." *Journal of Fluids and Structures* 23 (8): 1168–1188. doi:10.1016/j.jfluidstruct.2007.05.005.
- Lei, C., L. Cheng, and K. Kavanagh. 2001. "Spanwise Length Effects on Three-Dimensional Modelling of Flow over a Circular Cylinder." *Computer Methods in Applied Mechanics and Engineering* 190 (22): 2909–2923. doi:10.1016/S0045-7825(00)00272-3.
- Leonard, B. P. 1979. "A Stable and Accurate Convective Modelling Procedure Based on Quadratic Upstream Interpolation." *Computer Methods in Applied Mechanics and Engineering* 19 (1): 59–98. doi:10.1016/0045-7825(79)90034-3.
- Lourenco, L. M., and C. Shih. 1993. "Characteristics of the Plane Turbulent near Wake of A Circular Cylinder. A Particle Image Velocimetry Study." (Private Communication), Beaudan and Moin (1994).
- Lysenko, D. A., Ivar S. Ertesvåg, and Kjell Erik Rian. 2012. "Large-Eddy Simulation of the Flow over a Circular Cylinder at Reynolds Number 3900 Using the OpenFOAM Toolbox." *Flow, Turbulence and Combustion* 89 (4): 491–518. doi:10.1007/s10494-012-9405-0.
- Mittal, R., and S. Balachandar. 1997. "On the Inclusion of Three-Dimensional Effects in Simulations of Two-Dimensional Bluff-Body Wake Flows." In *Proceedings of the 1997 ASME Fluids Engineering Division Summer Meeting*, Vancouver, British Columbia, Canada, June 1997. New York: American Society of Mechanical Engineers (ASME).
- Ong, L., and J. Wallace. 1996. "The Velocity Field of the Turbulent Very near Wake of a Circular Cylinder." *Experiments in Fluids* 20 (6): 441–453. doi:10.1007/BF00189383.
- Parnaudeau, P., J. Carlier, D. Heitz, and E. Lamballais. 2008. "Experimental and Numerical Studies of the Flow over a Circular Cylinder at Reynolds Number 3900." *Physics of Fluids* 20 (8): 085101. doi:10.1063/1.2957018.
- Pereira, F. S., G. Vaz, L. Eça, and S. S. Girimaji. 2018. "Simulation of the Flow around a Circular Cylinder at Re=3900 with Partially-Averaged Navier-Stokes Equations." *International Journal of Heat and Fluid Flow* 69: 234–246. doi:10.1016/j.ijheatfluidflow.2017.11.001.
- Pereira, F. S., G. Vaz, and Eça. Luís 2015. "Flow past A Circular Cylinder: A Comparison between RANS and Hybrid Turbulence Models for A Low Reynolds Number." In *Proceedings of the ASME 2015 34th International Conference on Ocean, Offshore and Arctic Engineering. Volume 2: CFD and VIV*, St. John's, Newfoundland, Canada, May 31 - June 5 2015. New York: American Society of Mechanical Engineers.
- Rezaeiha, A., I. Kalkman, and B. Blocken. 2017. "CFD Simulation of a Vertical Axis Wind Turbine Operating at a Moderate Tip Speed Ratio: Guidelines for Minimum Domain Size and Azimuthal Increment." *Renewable Energy* 107: 373–385. doi:10.1016/j.renene.2017.02.006.
- Sidebottom, W., A. Ooi, and D. Jones. 2015. "A Parametric Study of Turbulent Flow past A Circular Cylinder Using Large Eddy Simulation." *Journal of Fluids Engineering* 137: 9. doi:10.1115/1.4030380.
- Smagorinsky, J. 1963. "General Circulation Experiments with the Primitive Equations." *Monthly Weather Review* 91 (3): 99–164. doi:10.1175/1520-0493(1963)091<0099:GCEWTP>2.3.CO;2.
- Tezduyar, T. E., and R. Shih. 1991. "Numerical Experiments on Downstream Boundary of Flow past Cylinder." *Journal of Engineering Mechanics* 117 (4): 854–871. doi:10.1061/(ASCE)0733-9399(1991)117:4(854).
- Versteeg, H. K., and W. Malalasekera. 2007. *An Introduction to Computational Fluid Dynamics the Finite Volume Method*. 2nd ed. England: Pearson Education Limited.
- Wang, Q., G. Zhang, W. Li, and L. Shi. 2020. "Numerical Simulation of Two-Way Fluid-Structure Interaction of Wind Loading on Buildings." *Journal of the Chinese Institute of Engineers* 43 (3): 225–240. doi:10.1080/02533839.2019.1708213.

Effect of boundary conditions and domain size on the turbulent flow characteristics over a circular cylinder

ORIGINALITY REPORT

24%

SIMILARITY INDEX

16%

INTERNET SOURCES

22%

PUBLICATIONS

4%

STUDENT PAPERS

MATCH ALL SOURCES (ONLY SELECTED SOURCE PRINTED)

2%

★ V M Molochnikov, N I Mikheev, A N Mikheev, A A Paereliy, N S Dushin, O A Dushina. "SIV measurements of flow structure in the near wake of a circular cylinder at $Re = 3900$ ", Fluid Dynamics Research, 2019

Publication

Exclude quotes Off

Exclude matches Off

Exclude bibliography On